# Supplementary Information for

## An Ion Concentration Polarization System that Exceeds Ohmic Scaling by Over One Order of Magnitude

Dayi Chen[a], Jin-Tae Kim[b], Leonardo P. Chamorro[b], Aaron T. Timperman[a*]
Correspondence to: atimperm@illinois.edu

**This PDF file includes:**

Reagents and Materials
Figures S1 to S12
Table S1 to S2.
Captions for Movies S1 to S4

**Other Supplementary Materials for this manuscript include the following:**

Movies S1 to S4

## Reagents and Materials

Benzophenone, acrylamide, N,N'-methylenebisacrylamide, 2-methyl-4'-(methylthio)-2-morpholinopropiophenone, 2-acrylamido-2-methylpropane sulfonic acid, and sodium phosphate monobasic were purchased from Sigma-Aldrich. Sodium phosphate was from VWR, and sodium bicarbonate was from EMD Millipore. Rhodamine 6G was obtained from Alfa Aesar. Alexa Fluor 488, Alexa Fluor 594 and FluoSpheres™ carboxylate-modified microspheres (1.0 µm, Nile Red fluorescent 535 nm / 575 nm, 2% solids) were purchased from ThermoFisher Scientific. Sylgard™ 184 Silicone Elastomer Kit was from Dow Silicones Corporation. SU-8 2025 photoresist is from Kayaku Advanced Materials, Inc. 10 nm pore size polyester (PET) membrane (23 µm thick with pore density of $4E09 \cdot cm^{-2}$) was ordered from it4ip S.A. (Belgium). 400 nm pore size PET membrane (12 µm thick with pore density of $2E06 \cdot cm^{-2}$) was obtained from Sterlitech Corporation. Flexible fused silica capillary tubing with 360 µm OD was from Molex. Water used in all the experiments was purified by Barnstead Nanopure Ultrapure Water Systems from Thermo Scientific (18.2 MΩ-cm). Si wafers were purchased from University wafers. Fisherbrand™ cover glasses, dimethyl sulfoxide (DMSO), acetone, and ethanol were from Fisher Scientific. All the chemicals were used without further purification.

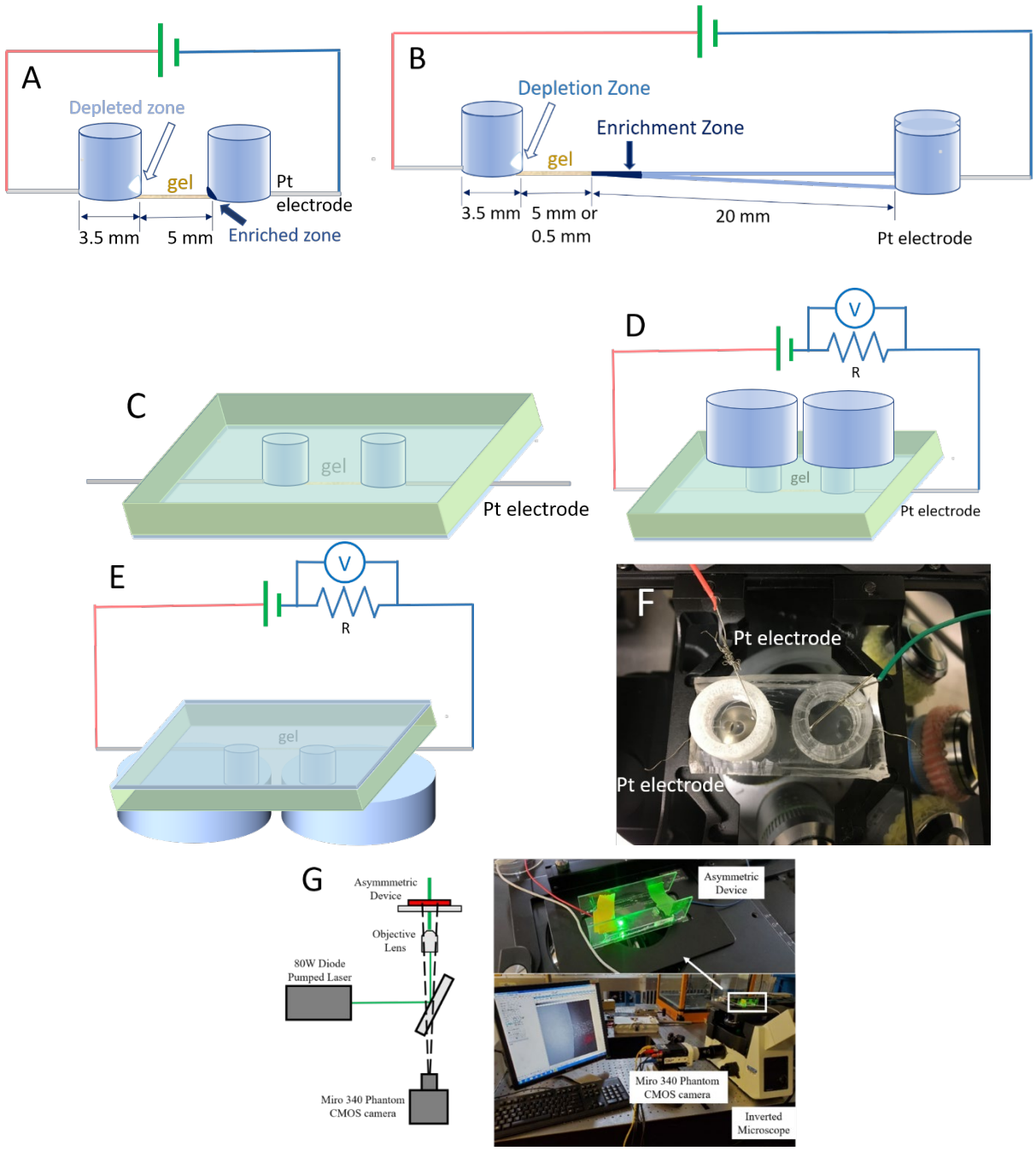


**Figure S1. The experimental set-up. (A)** Dimensions of short channel device. **(B)** Dimensions of long channel device. The microchannel bifurcation facilities cleaning and buffer replacement. **(C)** Schematic of the PDMS device. **(D)** Schematic of the current measurement circuit with upright orientation. **(E)** Schematic of the current measurement circuit with upside-down orientation. **(F)** Photo of a device with upright orientation on Leica SP8 UV/Visible laser confocal microscope. There are two pairs of Pt electrodes and only one pair is used at a time. Normally, the experiments were only run with the bottom electrode pair connected while the top pair was the electrode pair connected to test whether the electrode positions (shape of the electric field) would affect the depletion zone shape and current. **(G)** The experimental set-up of μ-PTV.

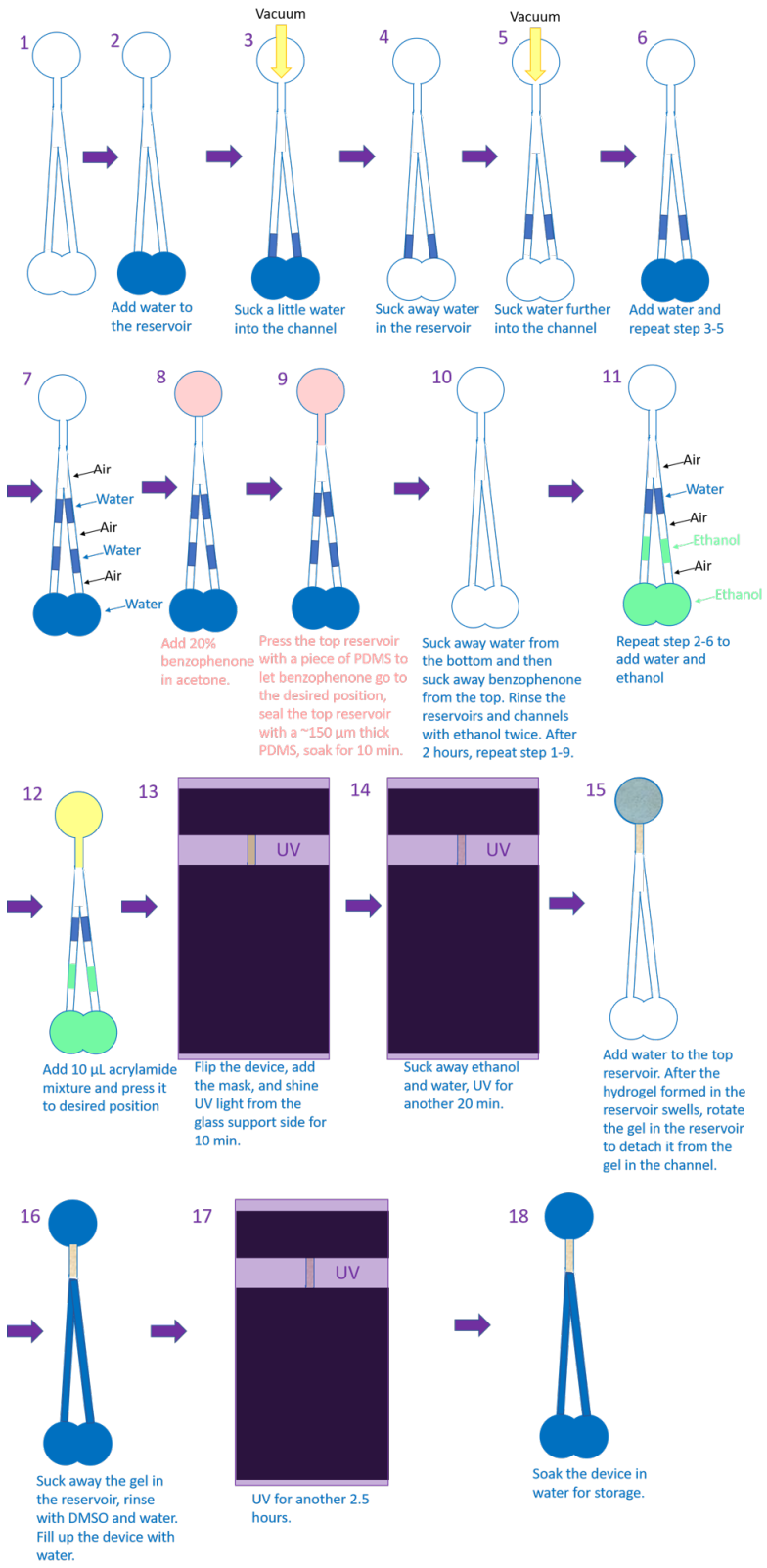


**Figure S2. Gel fabrication process for long microchannel devices** (the bottom merged reservoirs have ¼ diameter overlapped). The air and water in the channel were used to control the position of the gel. For 500 µm gel devices, step #13 and #14 are merged into one (UV for 30 min and then suck away ethanol and water), and if there is still extra gel in the reservoir in step #15, tweezers are used to cut the extra gel immediately after water is added. For short devices without long open channels, only step#9, #10, #12-18 are needed.

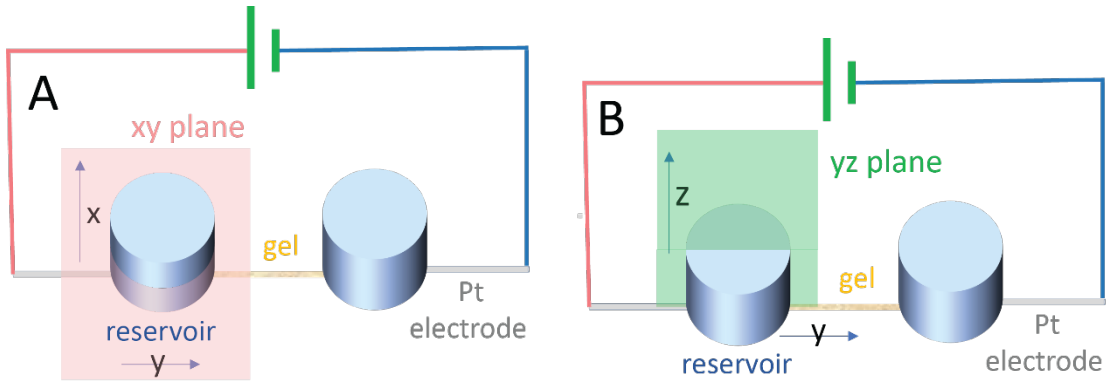


**Figure S3. Schematics illustrating the *x-y* and *y-z* planes used for acquisition of the confocal microscopy images. (A)** *x-y* plane. Scan range 1.55 mm × 1.55 mm with 10X objective lens and 600 µm × 600 µm with 20X objective lens, containing a bit of microchannel and partial reservoir. **(B)** *y-z* plane. Scan range 400 µm × 400 µm, containing only partial reservoir.

XYZT scans the x-y plane (Figure S3A) at a series of z positions (from the bottom of the reservoir – 0 µm to a certain height) as one stack, and the scan of a stack was repeated in the time sequence. YZT repeatedly scans the y-z plane at the microchannel center containing the nanoporous gel in the x-direction (Figure S3B) to build a time series of y-z images.

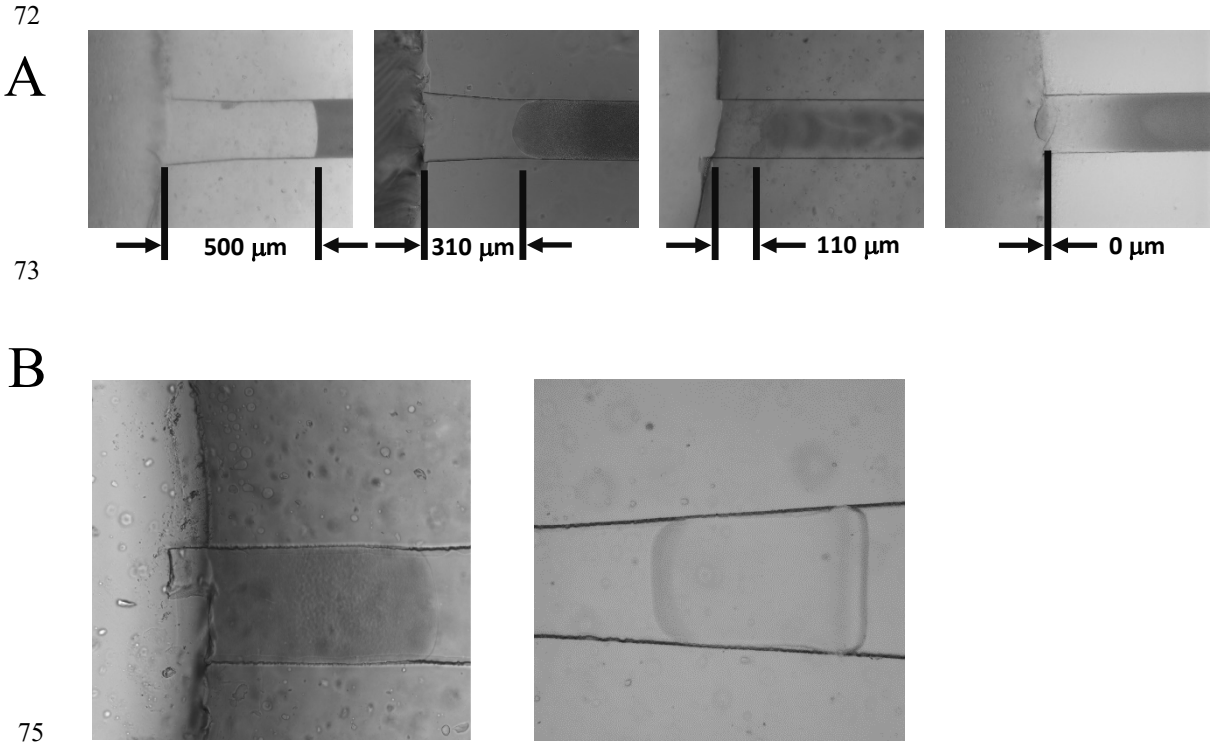


**Figure S4. Bright field images of devices filled with acrylamide gel. (A)** Images showing the distance between the 3D reservoir and the nanoporous gel that have open microchannel lengths of 500 µm, 310 µm, 110 µm, and 0 µm as labeled. **(B)** Images showing about 400 µm long acrylamide gel at the interface of the channel and the reservoir, and acrylamide gel in the middle of the channel.

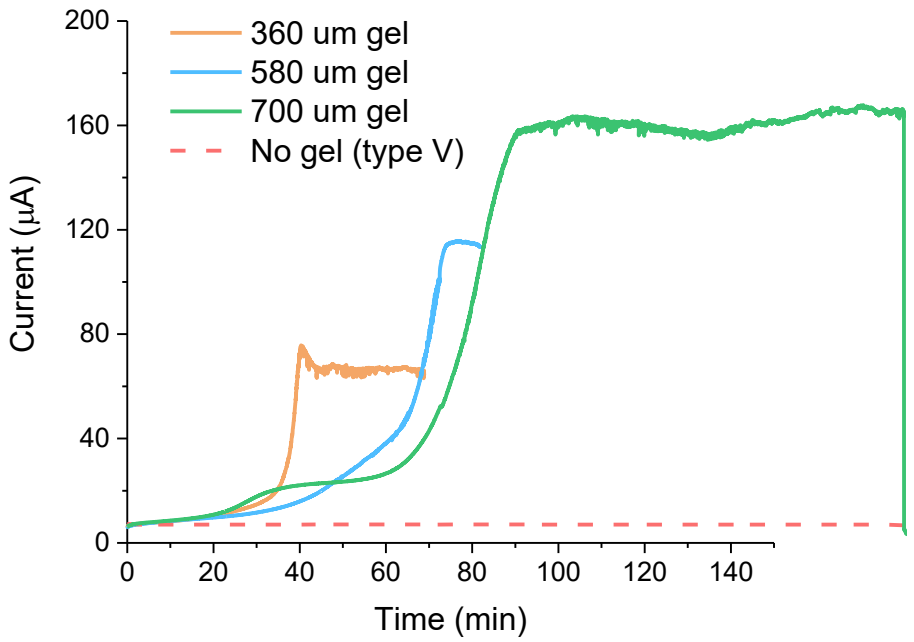


**Figure S5. Measured current as a function of time at 100 V with about 500 μm gel in type II devices.** All three devices have current exceeded one order magnitude of Ohmic current. When comparing to Ohm's law current limit, 360 μm one reaches 12-fold, 580 μm one reaches 19-fold, and 700 μm one reaches 23-fold. When comparing to no-gel control, 360 μm one reaches 10-fold, 580 μm one reaches 15-fold, and 700 μm one reaches 21-fold.

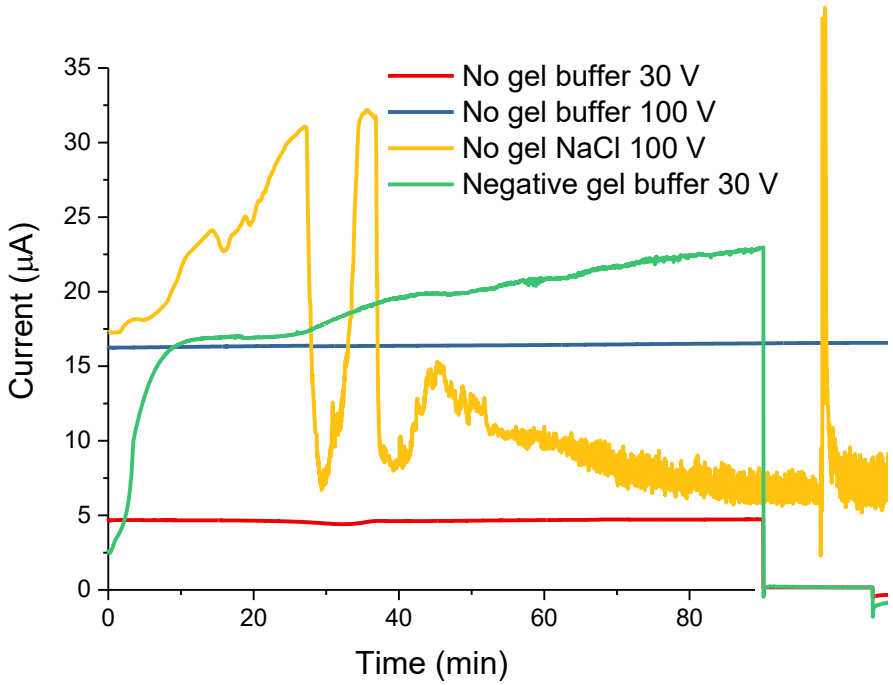


**Figure S6. Experiments that excluded water hydrolysis as the cause of current increase.** Water electrolysis at the electrodes can alter the conductivity of the electrolyte solution and introduce changes in current from unwanted variables. To insure pH stability of the buffer solution for 90 min, I-t plots were recorded for the symmetric devices with 10 mM buffer or NaCl solutions. The buffer consisted of 3 mM $Na_2HPO_4$, 2 mM $NaH_2PO_4$, and 5 mM $NaHCO_3$ at pH 7.5. The $NaHCO_3$ inhibits water hydrolysis. In the no gel cases the current is stable and an Ohmic relationship is observed between 30 and 100 V. With the unbuffered 10 mM NaCl solution, water electrolysis causes pH drift and bubbles that form on the electrodes produce additional current fluctuations.

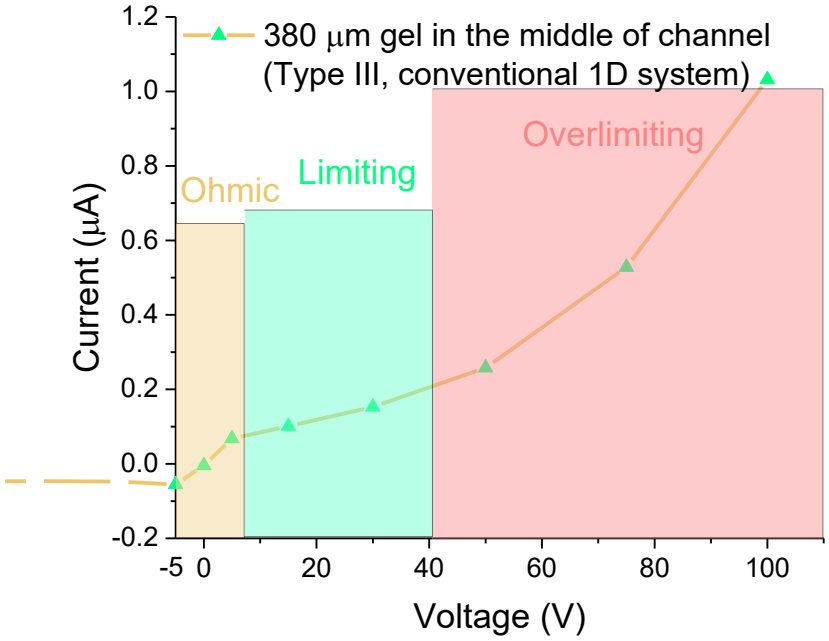


**Figure S7. I-V curve of conventional microchannel (1D) configuration with short gel in the middle of the channel (type III) from -5 V to 100 V.** The system shows Ohmic behavior in -5 V to 5 V range, limiting current from 5 V to ~ 30 V and overlimiting current above 30 V.

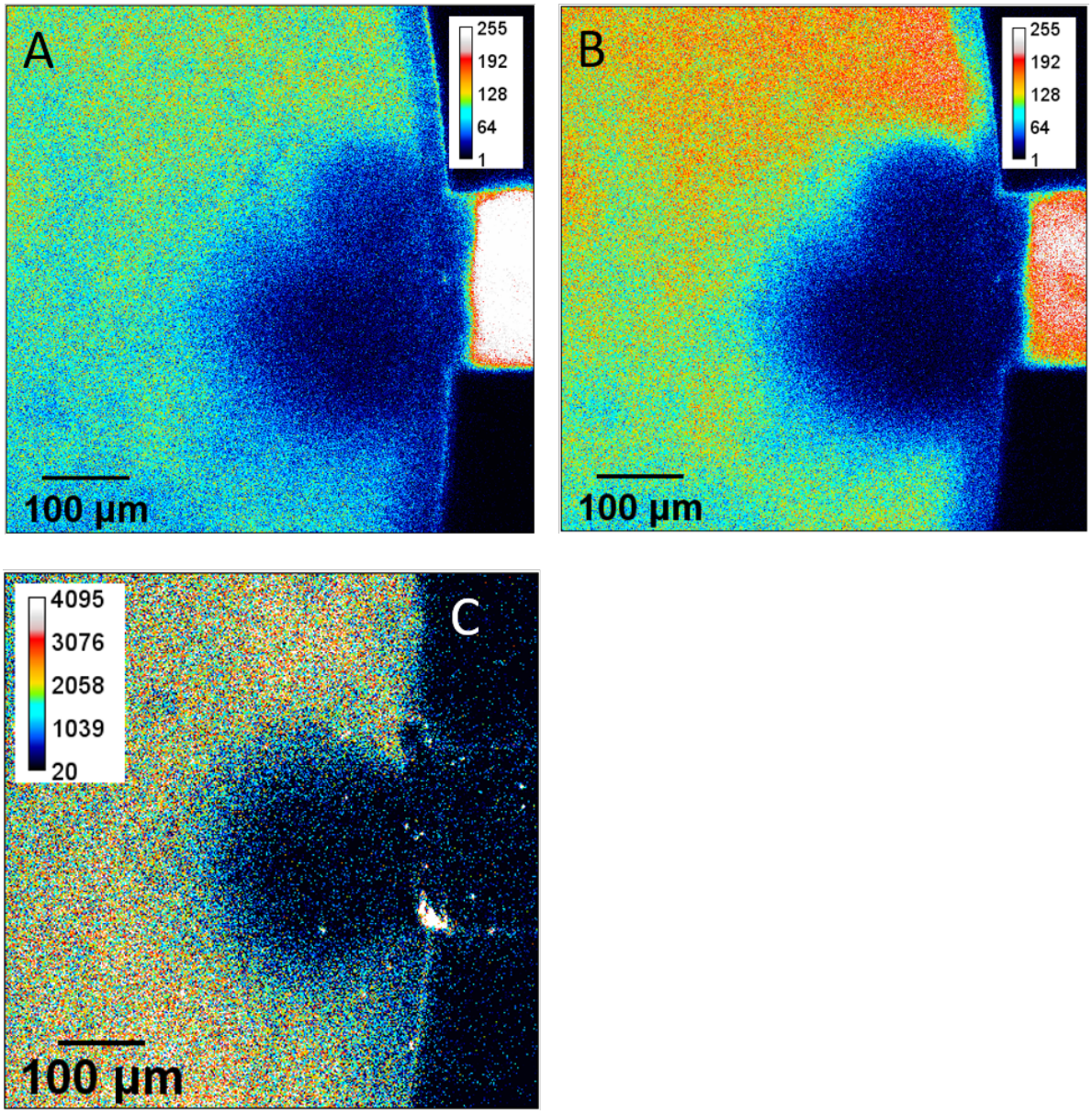


**Figure S8. Cation and anion tracer imaging near the CP depleted zone.** The simultaneous imaging of a cationic tracer **(A)** Rhodamine 6G, and **(B)** an anionic tracer Alexa Fluor 594 shows the exclusion of both the cation (counter-ion) and the anion (co-ion) from the CP depleted zone at a potential of 100 V. In **(C)** the imaging of only Alexa Fluor 594 confirms the exclusion of the co-ion from the negative nanoporous gel. Cross-talk between the two fluorescent channels in (A) and (B) causes the fluorescence intensity in the nanoporous gel in (B) that could be misinterpreted as indicating the presence of the co-ion in the nanoporous gel.

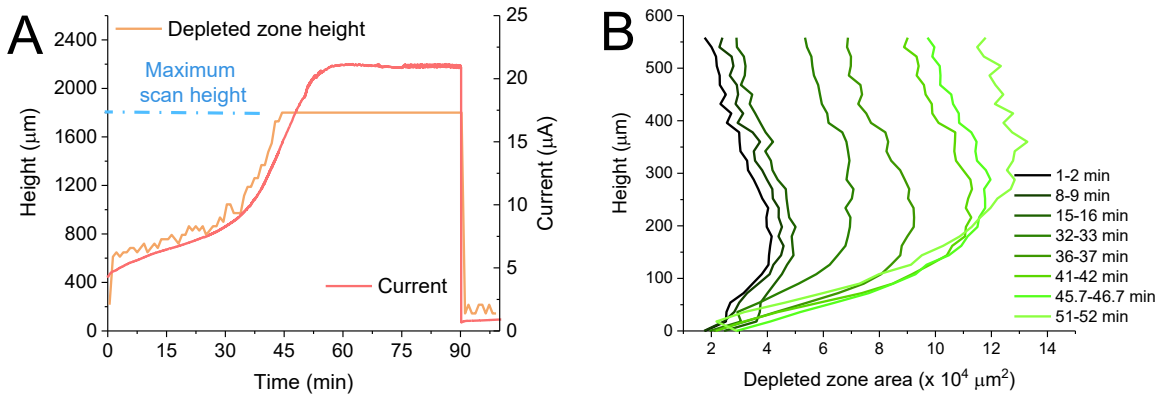


**Figure S9. CP Depleted zone shape change with time. (A)** The depleted zone height change with time and current. The depleted zone height is defined as the height at which 95% of the total depleted zone volume is reached. **(B)** The depleted zone area as a function of height (z) at different times. The vast majority of the depleted zone volume are far above the top of the negative nanoporous gel (36 μm).

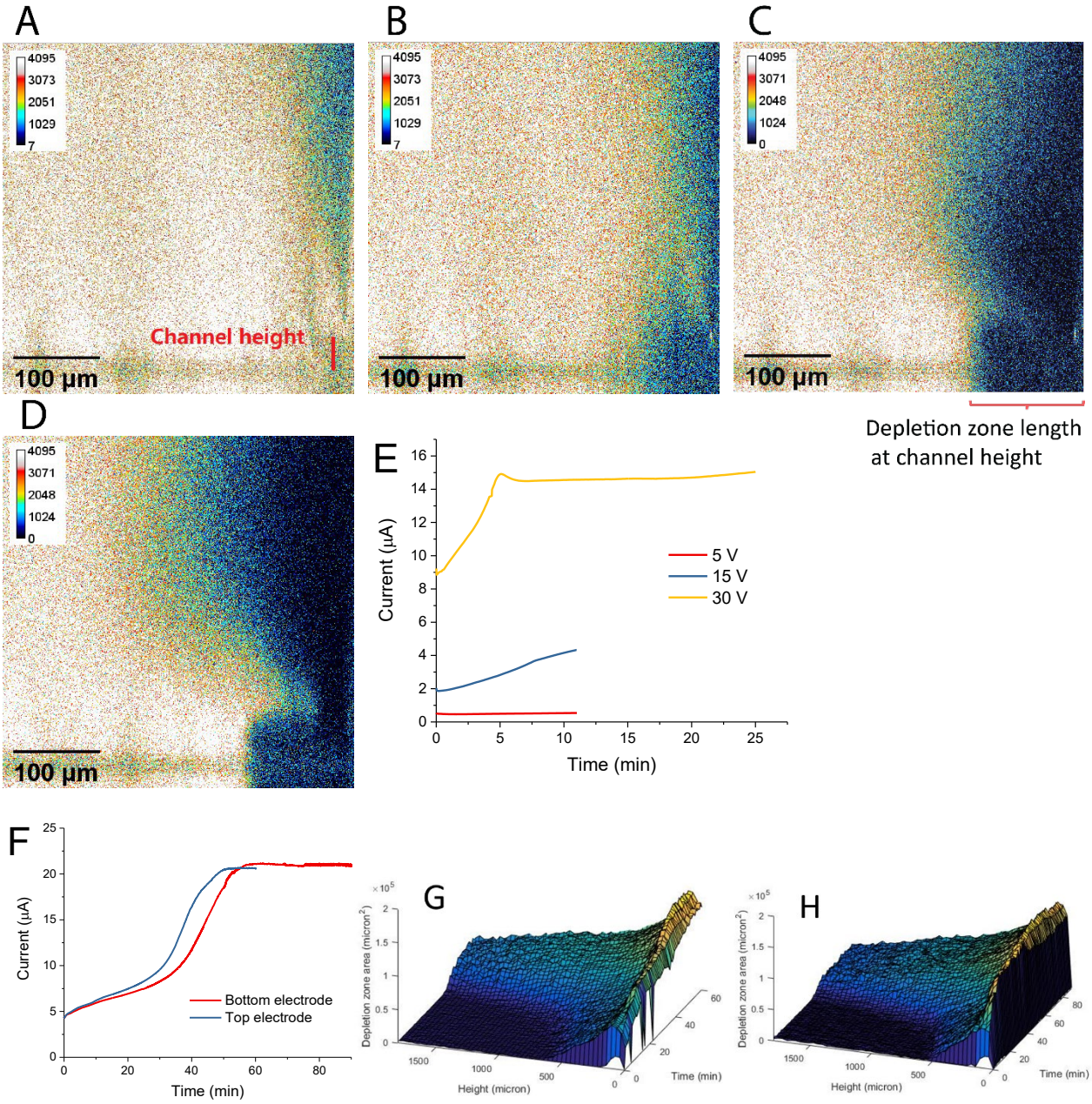


**Figure S10. CP depleted zone shape affected by the electric field.**

**(A)-(E)**: Vertical profile of the CP depleted zone shape as a function of voltage. The images were obtained with YZT scans. **(A)** 0 V at 10 min, **(B)** 5 V at 10 min, **(C)** 15 V at 10 min, **(D)** 30 V at 10 min, and **(E)** the corresponding I-t curves. 15 V and 30 V have the same depleted zone length at gel height (i.e. channel height) but their currents are three times different at 10 min. 5 V has its depleted zone not depleted as 15 V and 30 V, and its current is the smallest. The depleted zone length along at the gel height does not scale with voltage and current. **(F)-(H)**: Impact of electrode position on the CP depleted zone. **(F)** The current-time relations show little impact of the electrode position (the electrode positions are shown in FigureS1D). The depleted zone area as a function of height and time is nearly the same for the electrode at the **(G)** top of the reservoir and **(H)** bottom of the reservoir.

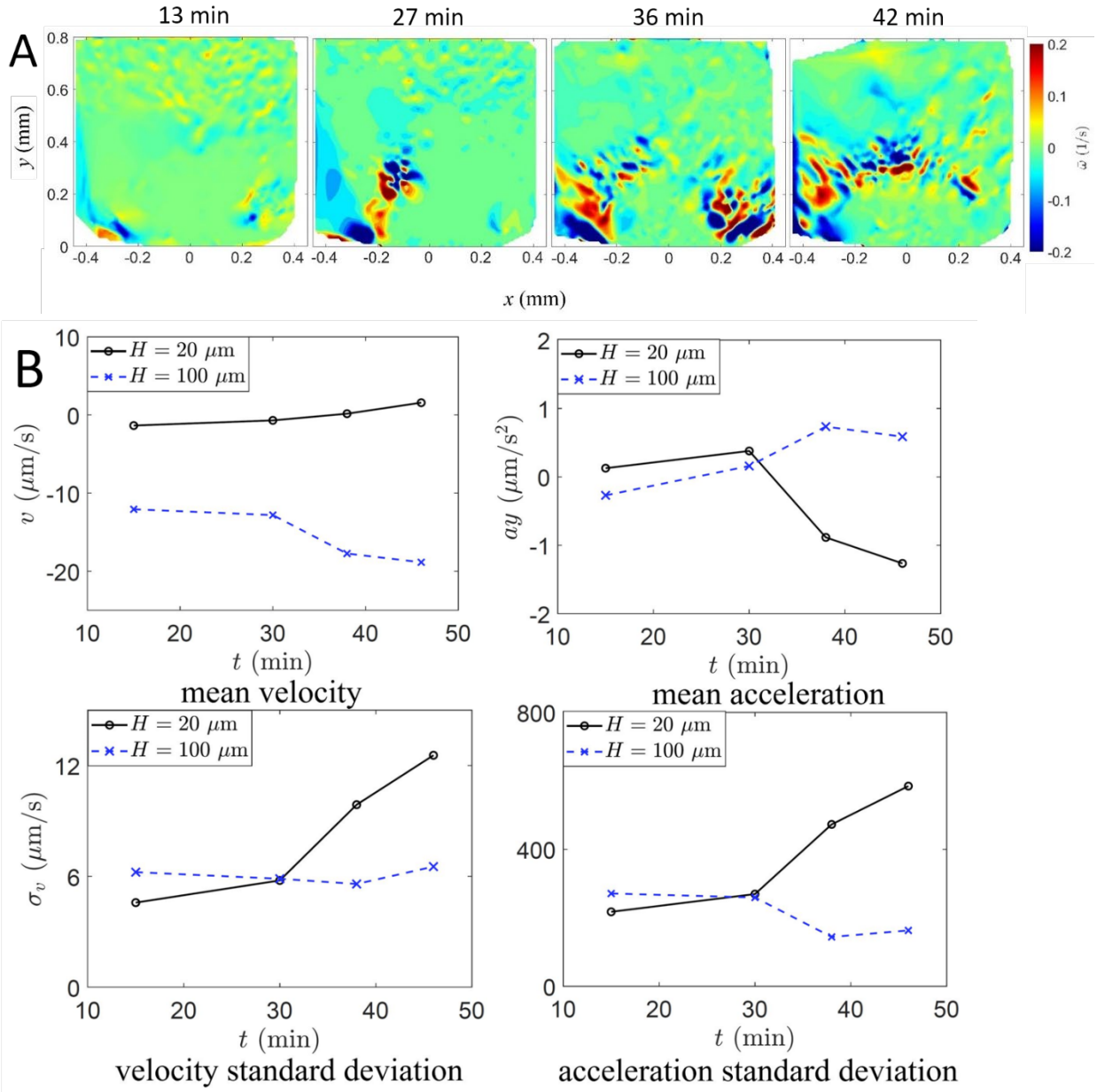
A
13 min
27 min
36 min
42 min
y (mm)
x (mm)
ω (1/s)
B
H = 20 μm
H = 100 μm
v (μm/s)
t (min)
mean velocity
ay (μm/s²)
mean acceleration
σv (μm/s)
velocity standard deviation
acceleration standard deviation

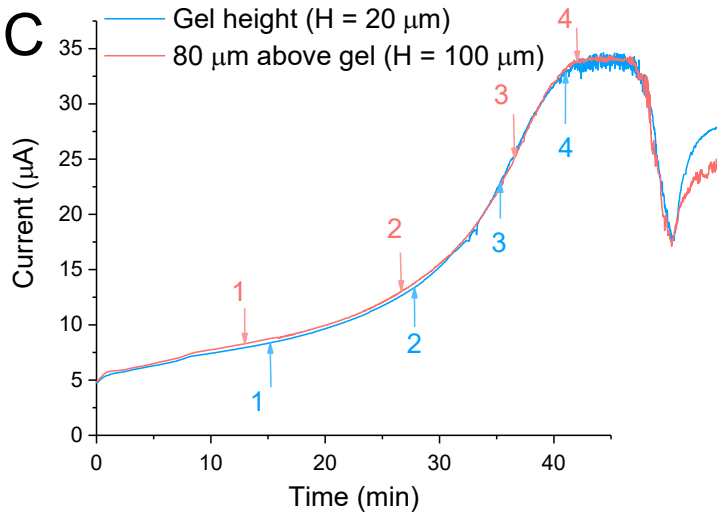
C
Gel height (H = 20 μm)
80 μm above gel (H = 100 μm)
Current (μA)
Time (min)

**Figure S11. Details of *x-y* plane μ-PTV. (A)** Average vorticity at gel height. The data extracted from Movie S2 at H = 20 μm was analyzed by: 1) interpolating the scattered trajectory data into the grid space, 2) determining the out of plane vorticity, and 3) averaging the temporal domain. **(B)** Mean velocity and acceleration of the flow in 3D macroscale reservoir extracted from Movie S2. The data are shown for two heights, gel height (H = 20 μm), and the other is 80 μm above the gel (H = 100 μm). **(C)** Current profiles of the μ-PTV experiments. Two series of μ-PTV experiments were performed at two heights. One is at gel height (H = 20 μm), and the other is at 80 μm above the gel (H = 100 μm). The numbers with the arrows indicate when the videos were recorded: (1) 15 min at H = 20 μm and 13 min at H = 100 μm, (2) 28 min at H = 20 μm and 27 min at H = 100 μm, (3) 35 min at H = 20 μm and 36 min at H = 100 μm, (4) 41 min at H = 20 μm and 42 min at H = 100 μm.

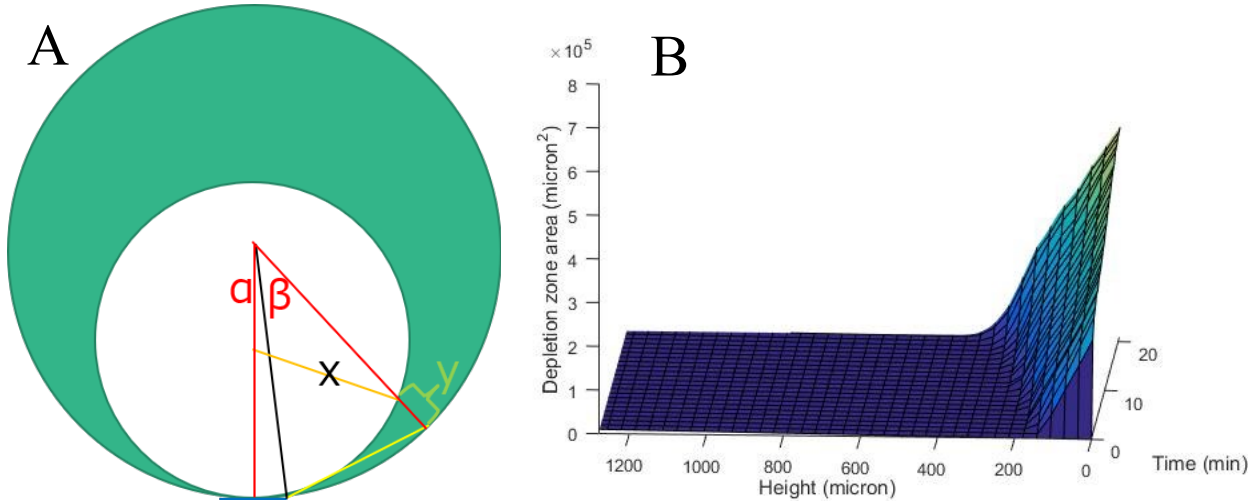


**Figure S12. Ion transport path with upside-down orientation.** (A). Calculation of the size of the depleted zone that would block the ion transport at *x*-*y* plane. The lengths are not drawn to scale. (B). Measured depleted zone area with upside-down orientation in the stacks of *x*-*y* plane along *z*-axis. The "Height" axis represents the distance between the *x*-*y* plane and PDMS ceiling.

Figure 3D shows a single *y*-*z* plane at the center of the gel. This plane contains the maximum length of the depleted zone at *x*-*y* plane (reach out of the field of view) and the maximum height of the depleted zone along *z*-axis. It doesn't reveal how the depleted zone occupies the space in other *x*-axis positions, especially the minimum length between the bulk solution and the nanoporous gel interface. Stacks of *x*-*y* plane images can show the whole picture of the depleted zone. Figure S10A represents the situation at *x*-*y* plane. The green circle represents the macro-reservoir, and the white circle represents the depleted zone. The red line represents the radius of the reservoir, 2 mm. The blue line represents the microchannel entrance of the nanoporous gel, and half of it is 0.1 mm. The yellow line represents the diffusion length of $Na^+$, 0.2 mm. The orange line represents the radius of the depleted zone, and its length is x. Length y represents the distance between the edge of the depleted zone and the edge of the reservoir. When y=0, the depleted zone blocks the ion transport path completely. Under current conditions, tan α can be calculated directly and cos β can also be calculated by Law of cosines. Thus, α equals 2.86° and β equals 5.73°. Length x can thus be calculated with cos(α+β) at different y. When y=100 μm, x=393 μm, representing a depleted zone area of $4.9\times10^5$ $\mu m^2$. When y=50 μm, x=626 μm, representing a depleted zone area of $1.23\times10^6$ $\mu m^2$. Because the diffusion length of $Na^+$ is 200 μm, *x*-*y* planes within height of (200+36) μm range in Figure S10B can supply $Na^+$ to nanoporous gel (36 μm height) if y >0. As shown in Figure S10B, all the depleted zone area measured are smaller than $1.23\times10^6$ $\mu m^2$, and only planes around gel height can reach $4.9\times10^5$ $\mu m^2$ when current is high, so there is still space between the depleted zone and the edge of the reservoir for ions to pass. The planes at PDMS ceiling and gel height extend the depleted zone area preferentially than other planes. However, when the ion transport is almost blocked by the depleted zone at these two planes, ions can still be transported from other planes within the $Na^+$ diffusion length. A very rough approximation is – when current is high and depleted zone area is large, with upright orientation, the ion flux can reach the nanoporous gel through both *x* and *y* dimensions, while with upside-down orientation, the ion flux can only pass through *z* dimension. Therefore, the ion flux to the nanoporous gel in the upside-down orientation is limiting compared to the upright orientation, but the maximum current doesn't drop too dramatically.

**Table S1.**

**Experimental details of confocal fluorescent imaging**

| Experiment | #1 | #2[3] | #3 | #4 | *y-z* μ-PTV |
|---|---|---|---|---|---|
| Fluorescent tracer | 8 μM Rhodamine 6G<br><br>5 μM Alexa Fluor 594 | 100 nM Alexa Fluor 594<br><br>500 nM Alexa Fluor 594 (Fig. 5A) | 100 nM Alexa Fluor 594 | 500 nM Alexa Fluor 594 | Carboxylate-modified 1.0 μm fluorescent microspheres ($7.2\times10^7$/mL) and 100 nM Alexa Fluor 594 |
| Scan type | XYZT | XYZT | YZT | XYZT<br>YZT | YZT |
| Scan size[1] (μm×μm) | 600 × 600 | 1550 × 1550<br><br>775 × 775 (Fig. 5A) | 400 × 400 | 1550 × 1550 (XYZT)<br>400 × 400 (YZT) | 400 × 400 |
| Spatial resolution (μm×μm) | 1.17 × 1.17 | 3.03 × 3.03<br><br>1.52 × 1.52 (Fig. 5A) | 0.783 × 0.783 | 3.03 × 3.03 (XYZT)<br>0.783 × 0.783 (YZT) | 0.783 × 0.783 |
| Scan range at z-axis in XYZT[2] (μm) | 50 | 1800<br><br>108 (Fig. 5A) | | 1332 | |
| Scan time | 39 s/stack | 53 s/stack<br><br>4.2 s/stack (Fig. 5A) | 1.49 s/frame | 39 s/stack (XYZT)<br>1.49 s/frame (YZT) | 0.72 s/frame |
| Corresponding figure and movie | Fig. 2F and Fig. S7 | Fig. 4, Fig. 5A and Fig. S8, Fig. S9F-H | Fig. S9A-D | Fig. 3 and Fig.S11B | Movie S1 |

1. It's x-y plane for XYZT scan and y-z plane for YZT scan.
2. All of the XYZT scans have z-axis step size of 36 μm except experiment#1, which is 5 μm.
3. The experiment of Fig. 5A used 20X objective lens (optical section ~2.5 μm).

**Table S2.**

**Steady state current at 5 V obtained after different high voltages**

| Initial high voltage | Current recorded within 10 s (μA) | Current recorded after 5 min (μA) |
|---|---|---|
| 100 V | 0.821 ± 0.122 | 0.968 ± 0.190 |
| 50 V | 0.838 ± 0.210 | 0.906 ± 0.212 |

The experiments were conducted in asymmetric devices after 100 V being applied for 90 min or 50 V being applied for 180 min. Each data point was averaged from three different devices. For each device, "current recorded within 10 s" averages 1-10 s current readings after the voltage was switched from a high voltage to 5 V, and "current recorded after 5 min" averages 10 s current readings 5 min later. The current increases slowly when 5 V is applied, therefore the current recorded after 5 min is a little larger than current recorded within 10 s.

There is no statistical difference between the data after 100 V and the data after 50 V, indicating the same steady state of the system was reached with different voltage. No gel case has current of 0.220 ± 0.009 μA at 5 V. The steady-state current summarized in this table is over 3-fold of it, same as the steady state of 100 V and 50 V.

This strategy, applying a high voltage to "activate the ion permselective element" and then switching to low voltage to inherit the active ion permselective element, will benefit low voltage applications greatly.

**Movie S1.**

*y-z* plane μ-PTV with negatively charged 1.0 μm fluorescent microspheres and 100 nM anionic Alexa Fluor 594 fluorescent dye in the buffer. The experiment was done in a short microchannel device at 30 V.

**Movie S2.**

*x-y* plane μ-PTV with negatively charged 1.0 μm fluorescent microspheres at two different heights, gel height (H = 20 μm) and 80 μm above gel height (H = 100 μm). The experiment was done in a long microchannel device, and 100 V was applied twice for the measurements at two heights.

**Movie S3**

Cations in 3D macro-reservoir moving to nanoporous gel. The experiment was done in a long microchannel device at 100 V with 200 nM cationic Rhodamine 6G fluorescent dye in the buffer. The end of the nanoporous gel extended a bit in the reservoir.

**Movie S4.**

*y-z* plane depleted zone dynamics with upside-down orientation. The experiment was done in a long microchannel device at 100 V with 500 nM anionic Alexa Fluor 594 fluorescent dye in the buffer.